Energy Storage Materials 22 (2019) 194–199

Contents lists available at ScienceDirect

Energy Storage Materials

journal homepage: www.elsevier.com/locate/ensm

# Self-healing electrostatic shield enabling uniform lithium deposition in all-solid-state lithium batteries

Xiaofei Yang [a], Qian Sun [a], Changtai Zhao [a], Xuejie Gao [a], Keegan Adair [a], Yang Zhao [a], Jing Luo [a], Xiaoting Lin [a], Jianneng Liang [a], Huan Huang [c], Li Zhang [b], Shigang Lu [b], Ruying Li [a], Xueliang Sun [a,*]

[a] Department of Mechanical and Materials Engineering, University of Western Ontario, London, ON, N6A 5B9, Canada
[b] China Automotive Battery Research Institute, Beijing, 100088, PR China
[c] Glabat Solid-State Battery Inc., 700 Collip Circle, London, ON, N6G 4X8, Canada

ARTICLE INFO

*Keywords:*
Solid polymer electrolyte
Solid-state batteries
Self-healing electrostatic shield
Li dendrite
Cesium

ABSTRACT

Poly(ethylene oxide) (PEO) based solid polymer electrolytes (SPEs) have been regarded as promising electrolytes for next-generation all-solid-state lithium batteries (ASSLBs). However, they have achieved limited cycling stability due to their inability to suppress Li dendrite growth. Herein, a self-healing electrostatic shield (SHES) is proposed to force uniform lithium deposition by introducing 0.05 M $Cs^+$. At this situation, the $Cs^+$ shows a lower reduction potential compared to the $Li^+$ reduction potential (1.7 M). During lithium deposition, the $Cs^+$ forms a positively charged electrostatic shield around the initial Li tips, which forces further deposition of lithium to adjacent regions of the anode and results in a dendrite-free Li deposition. With this in mind, the Li–Li symmetric cells can operate for 1000 and 500 h at current densities of 0.1 and 0.2 mA $cm^{-2}$, respectively, which are 10 times longer than $Cs^+$-free PEO electrolyte. Moreover, the Li/PEO-$Cs^+$/$LiFePO_4$ (LFP) cell achieves high capacity retention of 90% within 100 cycles at 0.5C and retains a high capacity of 113 mAh $g^{-1}$ at 0.8C, while short-circuits are observed for the Li/PEO/LFP cell, even at 0.2C. This strategy will generate substantial interest and shed light on the development of other dendrite-free SPEs and ASSLBs systems.

## 1. Introduction

All-solid-state lithium batteries have received increasing attention due to their higher energy density and improved safety compared with state-of-the-art liquid lithium-ion batteries [1–3].Among various solid-state electrolyte (SSE) systems, solid polymer electrolytes (SPEs) have been regarded as one of the most promising candidates for practical application in the terms of their flexibility, easy fabrication, low-density, good electrochemical stability, and excellent compatibility with lithium salts [4–10].

However, as one of the most widely used SSEs, PEO still suffers from low mechanical strength and the inability to prevent Li dendrite penetration, which significantly hinders its practical application [11–13]. In this regard, most efforts have been focused on improving the mechanical properties by adding (1) inorganic fillers and/or (2) crosslinking high strength polymers within the matrix of PEO. For instance, Cui and his workers reinforced the PEO electrolyte into a 3D interconnected silica-aerogel scaffold and significantly improved the modulus from 0.033 GPa (without silica-aerogel scaffold) to 0.43 GPa, enabling the Li–Li symmetric cells to run stably for 450 h at a current density of 0.05 mA $cm^{-2}$ (capacity:0.05 mAh $cm^{-2}$), which is 5 times longer than the pure PEO electrolyte [14]. Zhang and his coworkers introduced the Garnet-type $Li_{6.75}La_3Zr_{1.75}Ta_{0.25}O_{12}$ (LLZTO) with an ultra-high shear modulus of 55 GPa into the PEO system. The results showed that the LLZTO filler can significantly improve the mechanical strength as well as induce a uniform distribution of lithium ions, thus contributing to a dendrite-free lithium deposition. In this regard, the Li–Li symmetric cells could operate for 400 h at a current density of 0.1 mA $cm^{-2}$ [15]. Alternatively, cross-linking high strength polymers within the PEO matrix has been demonstrated to be another effective strategy. Guo's group photo-polymerized a branched acrylate onto the ion-conductive PEO matrix and achieved high mechanical strength (ca. 12 GPa). The results showed that such a high modulus is capable of suppressing Li dendrites and could realize stable Li–Li symmetric cell cycling performance of 130 h at a

* Corresponding author.
*E-mail address:* xsun9@uwo.ca (X. Sun).

https://doi.org/10.1016/j.ensm.2019.07.015
Received 3 May 2019; Received in revised form 3 July 2019; Accepted 9 July 2019
Available online 13 July 2019

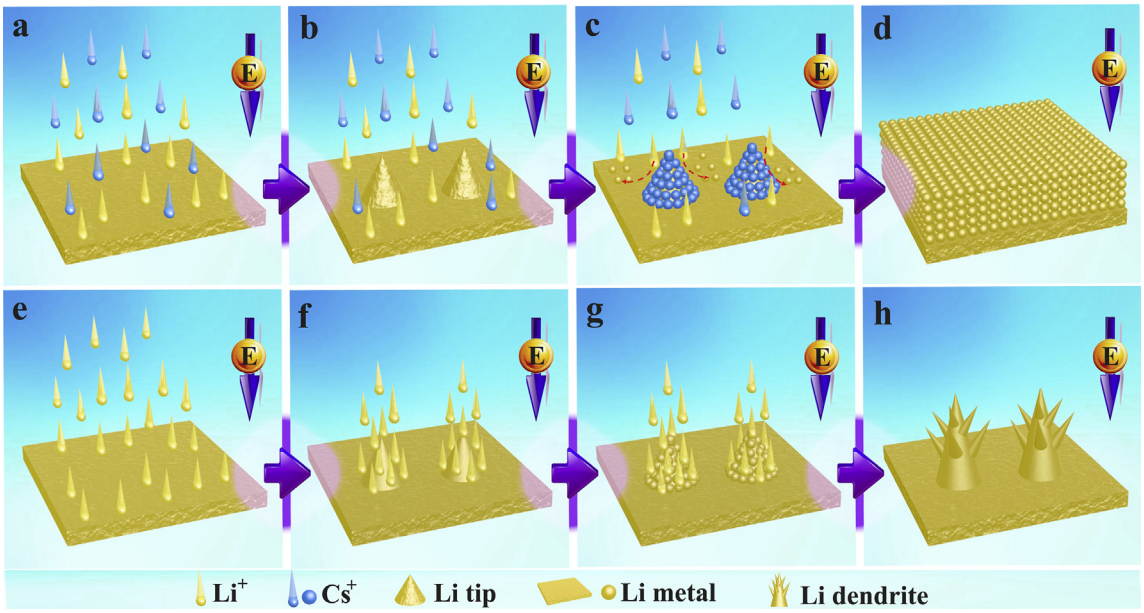


**Scheme 1.** Illustration of the Li deposition process for (a~d) PEO-$Cs^+$ electrolyte and (e~h) conventional pure PEO electrolyte.

current density of 4 mA $cm^{-2}$ (capacity: 1 mAh $cm^{-2}$) [16]. Despite the achievements, the high density of inorganic fillers will no doubt affect the energy density of ASSLBs and the cross-linking of polymers need relatively complicated processes. Moreover, our previous work showed that a low concentration of inorganic fillers such as 20 vol%, is insufficient to suppress the Li dendrites. Moreover, a high concentration of inorganic fillers (such as 80 vol%), also leads to interface problem as well as worse ionic conductivity [17].

Electrolyte additives were also reported to stabilize the anode surface and have been proved to be effective in suppressing Li dendrite growth. $LiNO_3$ and $Li_3N$ have been demonstrated to significantly improve the stability of the Li anode surface. The Li–Li symmetric cell with $LiNO_3$ and $LiN_3$ additives can enable stable operation for over 300 h and 650 h at a current density of 0.1 mA $cm^{-2}$ (capacity:0.2 mAh $cm^{-2}$), respectively, which is superior to that of pure PEO electrolytes (a short circuit occurs after 100 h) [18]. However, the consumption of such Li salt additives by forming a solid-electrolyte interface (SEI) during Li deposition is problematic, and the suppression of Li dendrites is not sustainable. Moreover, the volume and shape change of the Li anode during cycling may continuously consume these additives.

Recently, Zhang and co-workers proposed a novel strategy of building an electrostatic shield around the lithium surface to prevent the dendrite growth in liquid electrolytes [19]. $Cs^+$ was added into the electrolytes, contributing to the significantly improved cycling life. Herein, inspired by Zhang's work in the liquid electrolyte [19], a self-healing electrostatic shield (SHES) strategy is proposed to enable uniform Li deposition in a PEO-based ASSLBs system, aimed at solving the aforementioned lithium dendrite issue.

## 2. Experimental section

### 2.1. Synthesis of PEO and PEO-$Cs^+$ electrolytes

The PEO electrolytes with or without $Cs^+$ additive were prepared by a solution casting method. Firstly, the mixed solution of PEO polymer ($M_w$: 1000000, 0.60 g), bis(trifluoromethylsulfonyl) imide (LiTFSI) salt (0.24 g) with or without $CsClO_4$ (around 6 mg) were dissolved in 20 mL acetonitrile and vigorous stirring overnight, where the EO/Li ratio was controlled as 16/1. Then, the solution was cast in a polytetrafluoroethylene (PTFE) dish and dried at 60 °C for 24 h in vacuum. The obtained polymer membrane without $CsClO_4$ was labeled as PEO electrolyte. The obtained polymer membrane with $CsClO_4$ was labeled as PEO-$Cs^+$ electrolyte.

### 2.2. Synthesis of LFP electrodes

The LFP electrodes were fabricated by a blade casting technique. Typically, the LFP powder, acetylene black and PEO/LITFSI (EO/Li = 16/1) composite were dissolved in acetonitrile with a weight ratio of 8:1:1 to form a slurry and then coated onto aluminum (Al) foil, where the PEO ratio is 7.1 wt% in the cathode. After that, the Al foil coated with slurry was directly dried in a 60 °C oven overnight. The obtained cathodes were labeled as LFP electrodes.

### 2.3. Materials characterization

The morphology, structure, and composition of the electrolyte and electrode were characterized by SEM (Hitachi S-4800 and Hitachi S-3400).

### 2.4. Electrochemical measurements

The electrochemical performance of Li-LFP batteries and Li–Li symmetrical cells were tested with CR2032 coin cells, constructed in an Ar-filled glove box. The LFP cathode and Li anode were separated by PEO or PEO-$Cs^+$ electrolytes. The charge-discharge tests were carried out using a LAND CT-2001A system with voltages arrange from 2.7 V to 4.0 V at an operating temperature of 60 °C. Constant current densities were applied to the electrodes during repeated Li stripping/plating process.

The ionic conductivity of the electrolytes is determined by EIS measurement utilizing stainless steel | electrolyte | stainless steel symmetric cells with controlled temperature. The electrochemical stability window was examined by stainless steel | electrolyte | Li metal cells.

## 3. Result and discussion

As shown in Scheme 1, due to the defects on the Li anode surface and the non-uniform charge distribution during the initial platting process (Fig. S1), Li will be deposited on the substrate and unavoidably form dendritic tips under the applied voltage (Scheme 1b and Scheme 1f). The Li tips show higher activity towards Li nucleation rather than on smooth

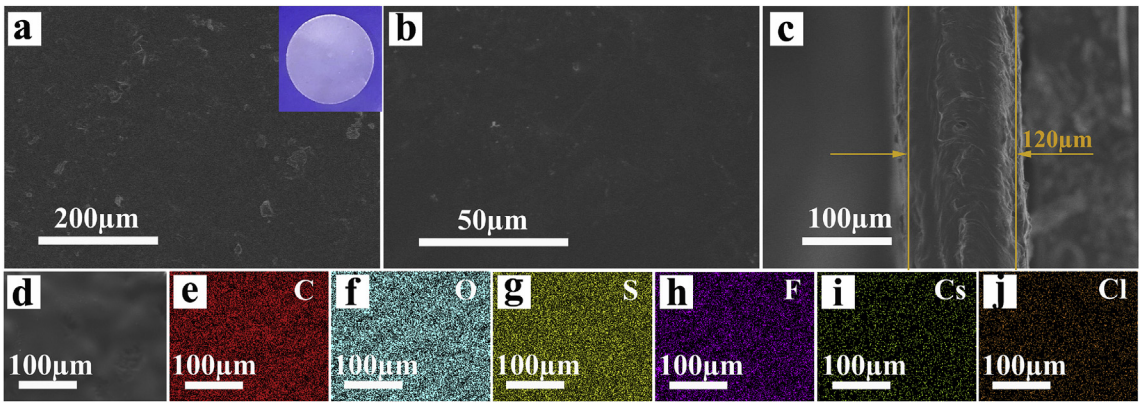


**Fig. 1.** (a)~(b) Surface and (c) cross-sectional morphology of PEO-$Cs^+$ electrolyte at different magnifications. (d) SEM images and corresponding elemental mappings of (e) C, (f) O, (g) S, (h) F, (i) Cs and (j) Cl. Inset of (a) is the optical image of PEO-$Cs^+$ electrolyte.

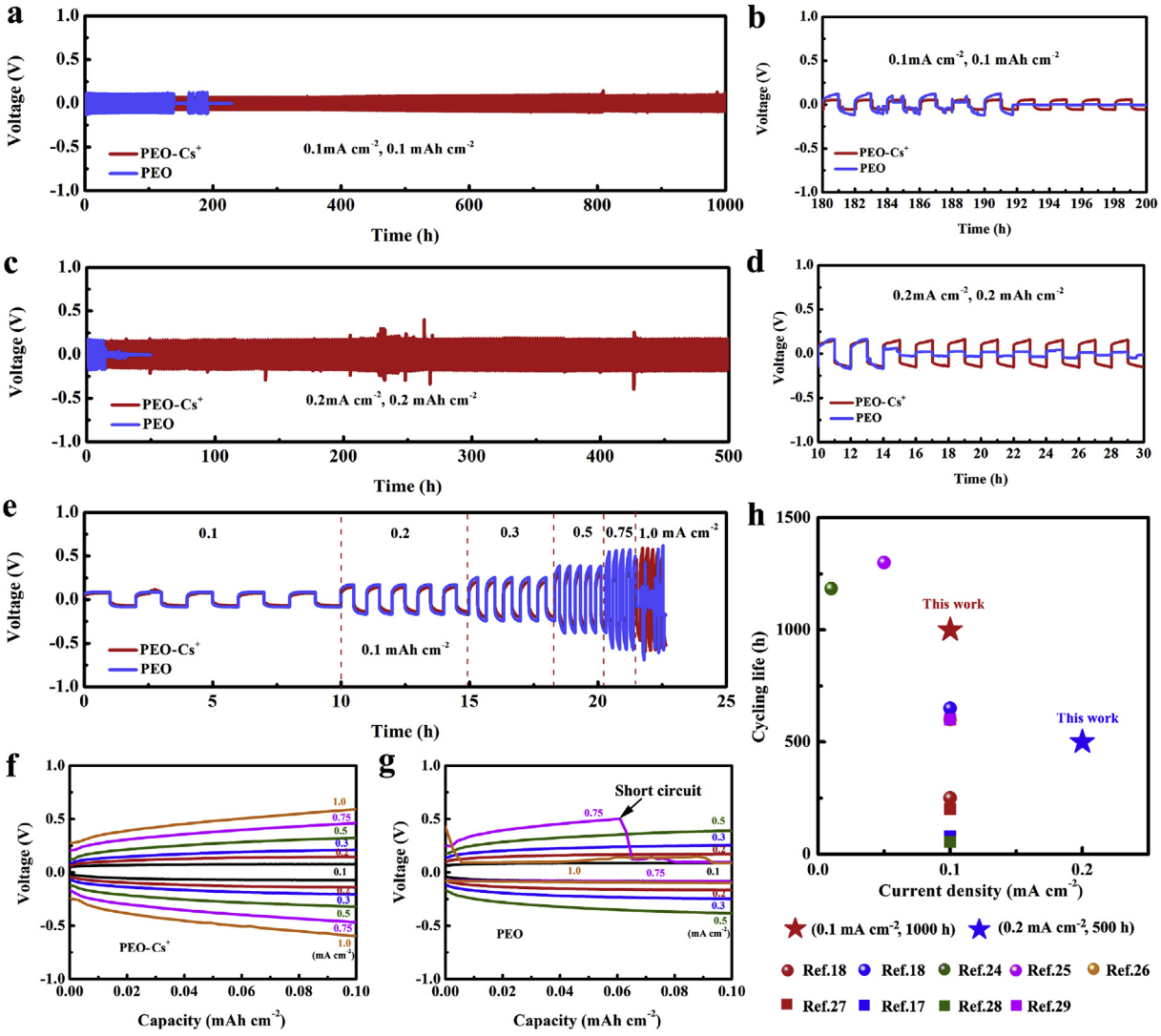


**Fig. 2.** Comparison of the cycling stability of the Li–Li symmetrical cells assembled with PEO-$Cs^+$ and PEO electrolyte at (a–b) 0.1 mA $cm^{-2}$ (capacity: 0.1 mAh $cm^{-2}$) and (c–d) 0.2 mA $cm^{-2}$ (capacity: 0.2 mAh $cm^{-2}$). (e) Rate performance of the Li–Li symmetrical cells assembled with PEO-$Cs^+$ and PEO electrolytes at various current densities of 0.1–1 mA $cm^{-2}$ with a limited capacity of 0.1 mAh $cm^{-2}$. Relatively plating/stripping profiles of (f) PEO-$Cs^+$ electrolyte and (g) PEO electrolyte. (h) Comparison of the recently reported plating/stripping performances of SPEs-based Li–Li symmetric cells with respect to current density and cycling life.

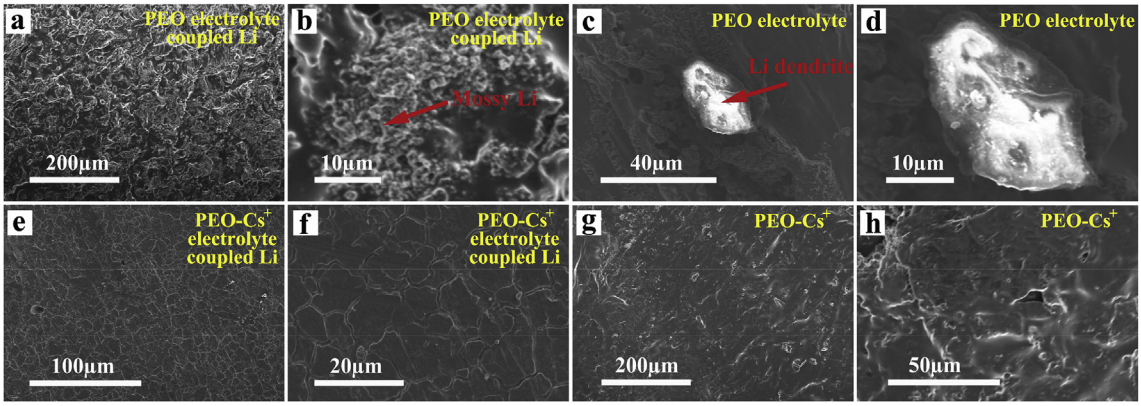


**Fig. 3.** SEM images of (a)~(b) PEO electrolyte-based Li and (c)~(d) PEO electrolyte after 100 h; SEM images of (e)~(f) PEO-$Cs^+$ electrolyte based Li and (g)~(h) PEO-$Cs^+$ electrolyte after 100 h.

regions of the anode, resulting in Li dendrite growth in conventional PEO-based SPEs (Scheme 1g ~ h). In contrast, when 0.05 M $Cs^+$ is introduced (~0.7 wt% in the SPE, labeled as PEO-$Cs^+$ electrolyte), the $Cs^+$ exhibits a lower reduction potential (0.05 M, −3.103 V) compared to that of Li ions (1.7 M $Li^+$ in PEO electrolyte (EO/Li = 16/1), −3.026 V) according to the Nernst equation [19]. In this case, the $Cs^+$ will accumulate on the tips and form a positively charged shield instead of depositing on the tips (Scheme 1c). Benefiting from the charge repulsion between the $Cs^+$ and $Li^+$, the incoming $Li^+$ will be forced to deposit at the adjacent regions of the anode until a smooth and uniform Li deposition layer is formed (Scheme 1d). Considering that the $Cs^+$ will not be consumed during the long term plating/stripping processes, excellent capability in inhibiting the Li dendrite growth can be expected. Additionally, the extremely low concentration of $Cs^+$ will not increase the cost of fabrication significantly or lower the energy density. In this regard, SHES forced uniform Li deposition strategy by introducing an ultra-low concentration of $Cs^+$ additive is a promising way to develop dendrite-free SPEs-based ASSLBs.

The PEO and PEO-$Cs^+$ electrolytes are synthesized by solvent-casting as described in the experimental section. The morphology and structure of the as-prepared PEO and PEO-$Cs^+$ electrolytes are firstly investigated by scanning electron microscopy (SEM). As shown in Fig. 1 and Fig. S2, both the PEO and PEO-$Cs^+$ SSEs exhibit a flat surface with a thickness of around 120 and 115 μm, respectively. The uniformly dispersed Cs and Cl elemental mappings are detected in the PEO-$Cs^+$ electrolyte, indicating that the $Cs^+$ is well-dispersed in the PEO matrix, which is beneficial for fabricating a uniform SHES to suppress Li dendrite growth.

In order to exclude the other possible influencing factors that would affect the following electrochemical performance testing, both the ionic conductivity and electrochemical stability window of the two electrolytes are investigated. As shown in Fig. S3, both of the electrolytes exhibit a similar ionic conductivity of $1.9 \times 10^{-4}$ S $cm^{-1}$ at an operating temperature of 60 °C and an electrochemical stability window of 4.35 V, which coincide well with recently reported pure PEO electrolytes [20,21]. In other words, the PEO-$Cs^+$ electrolyte shows similar physical and chemical properties compared with that of pure PEO electrolyte.

The electrochemical stability of the PEO and PEO-$Cs^+$ electrolytes is investigated by the Li–Li symmetrical cells at an operating temperature of 60 °C. The Li–Li symmetrical cells are assembled with SPEs sandwiched by two Li foils (diameter: 1.0 cm) and the current densities are controlled as 0.1 mA $cm^{-2}$ and 0.2 mA $cm^{-2}$ (charge/discharge time: 1 h), respectively. As shown in Fig. 2a, due to the similar ionic conductivity of the PEO and PEO-$Cs^+$ electrolytes, both of the two electrolytes exhibit a similar initial overpotential of 70 mV because of the mass-transfer resistance [22,23]. The difference between the two electrolytes are observed during Li plating/stripping. The cell assembled with PEO electrolyte displays intermittent short-circuiting after 140 h. After 192 h at 0.1 mA $cm^{-2}$, complete short-circuiting is observed, which can be attributed to the poor mechanical properties of the PEO electrolyte as well as non-uniform Li deposition (Fig. 2b). In contrast, PEO-$Cs^+$ electrolyte exhibits very stable performance in Li–Li symmetrical cells, where the overpotential only slightly increases to 97 mV after 1000 h of stripping and plating at 0.1 mA $cm^{-2}$.

When further increasing the current density to 0.2 mA $cm^{-2}$, the overpotentials of the cells assembled with the PEO and PEO-$Cs^+$ electrolyte both increase to around 160 mV (Fig. 2d). Due to the more serious Li dendrite growth at high current densities and high areal capacities, the cell assembled with the PEO electrolyte can only stably run for 15 h at 0.2 mA $cm^{-2}$. After that, the overpotential is sharply reduced to around 0 V and a short circuit is observed (Fig. 2c). Promisingly, the PEO-$Cs^+$ electrolyte achieves stable plating/stripping performance at an elevated current density of 0.2 mA $cm^{-2}$ for 500 h with an overpotential of around 185 mV. Such excellent electrochemical performance is superior to recently reported SPEs (not including inorganic fillers), listed in Table S1 and Fig. 2h in terms of cycling life and current density [17,18,24–29].

Meanwhile, the rate performance is also investigated with elevated current densities from 0.1 to 1 mA $cm^{-2}$, while the capacity is controlled at a constant value of 0.1 mAh $cm^{-2}$ (Fig. 2e). The results demonstrate that the PEO-$Cs^+$ electrolyte shows very stable performance during the whole stripping/plating process with the overpotential increasing from 73 mV (0.1 mA $cm^{-2}$) to 589 mV (1.0 mA $cm^{-2}$, Fig. 2f). In contrast, for the PEO electrolyte, a short-circuit is observed when the current density increases to 0.75 mA $cm^{-2}$ (Fig. 2g). Considering the same Li foil is used in the two cells, the difference in suppressing Li dendrite can be attributed to the different electrolytes.

To understand the behavior of Li stripping and plating within different SPEs, the Li–Li symmetrical cells operated at a current density of 0.2 mA $cm^{-2}$ (capacity: 0.2 mAh $cm^{-2}$) after 100 h are disassembled and the morphology of SSEs and Li anode are checked by SEM (Fig. 3). As shown in Fig. 3a~b, after cycling, large amounts of uniformly dispersed mossy Li are observed on the surface of Li anode when coupled with pure PEO electrolyte. Moreover, some large observable Li dendrites with a diameter of 10–20 μm, shown in Fig. 3c ~ d and Fig. S4, are detected on the surface of the PEO electrolyte. In order to confirm that these micro-sized fragments are Li, the electron beam is focused on the area for 10 min. As can be seen, the morphology of the point gradually changes (Fig. S4), which mainly attributed to the melting of Li under the high-energy electron beam. These large Li dendrites are the main reason leading to the low Coulombic efficiency (CE) of the lithium batteries as well as severe safety risks [30,31]. Interestingly, for the PEO-$Cs^+$ electrolyte-coupled Li anode, as exhibited in Fig. 3e ~ f, there is no Li dendrite or mossy Li that can be observed and a flat surface appears after platting/stripping for 100 h, which is in good agreement with our design. Moreover, the PEO-$Cs^+$ electrolyte maintains its original morphology and

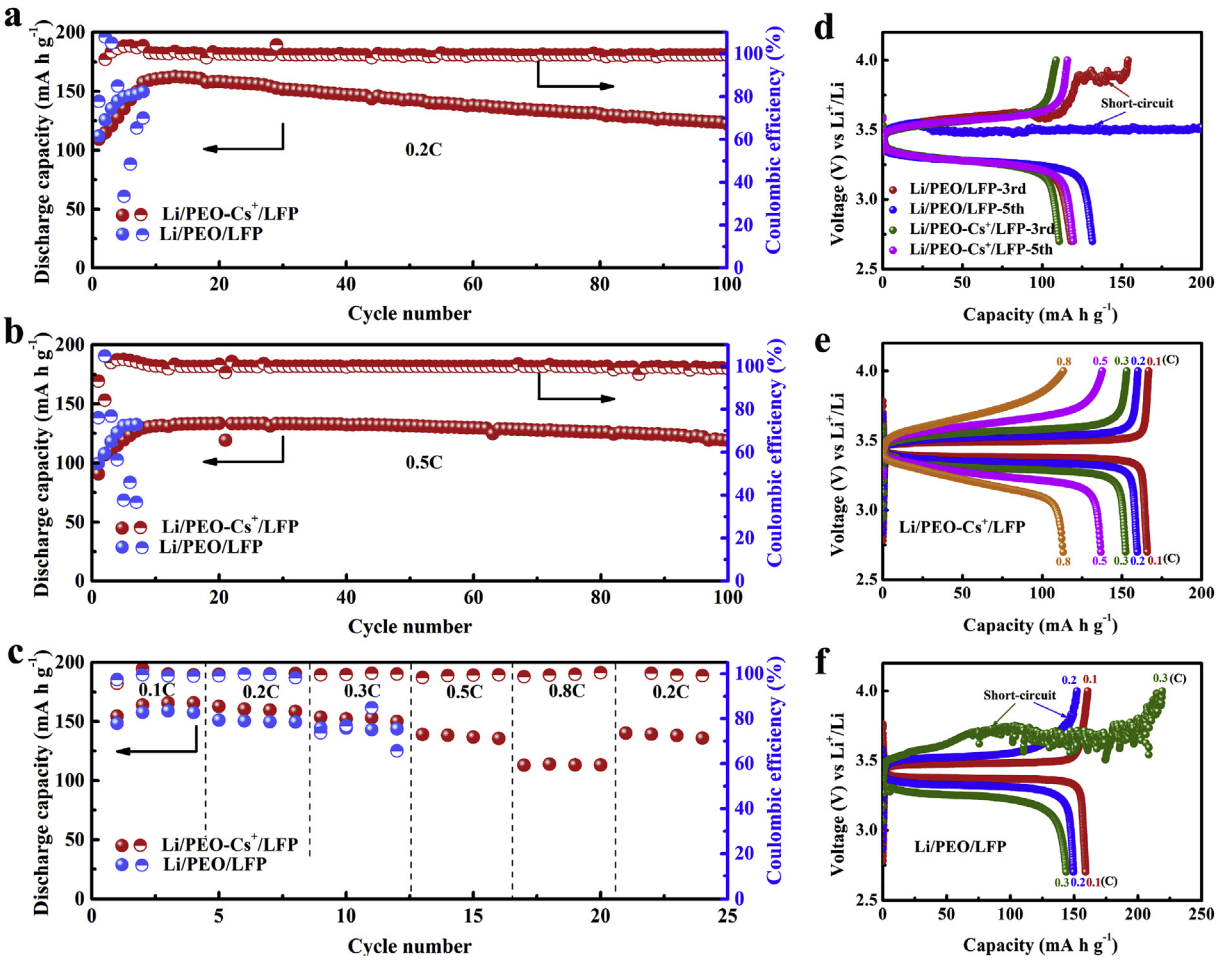


**Fig. 4.** Cycling performance at (a) 0.2C and (b) 0.5C of the Li/PEO/LFP and Li/PEO-$Cs^+$/LFP cells. (c) C-rate performance of the Li/PEO/LFP and Li/PEO-$Cs^+$/LFP cells at various C-rate from 0.1C to 0.8C. (d) Charge-discharge profiles of Li/PEO/LFP and Li/PEO-$Cs^+$/LFP cells at 0.5C for the 3rd and 5th cycles. Charge-discharge profiles of (e) Li/PEO-$Cs^+$/LFP and (f)Li/PEO/LFP cells at various C-rate. (All of the cells are tested at an operating temperature of 60 °C.)

also no mossy/dendritic Li can be observed (Fig. 3g ~ h). The strong capability of the PEO-$Cs^+$ electrolyte in inhibiting dendrite growth benefits from the low concentration of $Cs^+$ with low reduction potential that enables uniform Li deposition.

The difference in Li dendrite suppression capabilities of the PEO and PEO-$Cs^+$ electrolytes are verified by the electrochemical performance of Li-LFP full ASSLBs with LFP as the cathode material. The cycling performance of Li-LFP ASSLBs assembled with PEO and PEO-$Cs^+$ electrolytes, labeled as Li/PEO/LFP and Li/PEO-$Cs^+$/LFP, respectively, are tested at galvanostatic charge/discharge C-rates of 0.2C and 0.5C between 2.7 V and 4.0 V. As shown in Fig. 4a, in the first 10 cycles, both of the two cells present an activation process with a gradually increasing discharge capacity, which can be attributed to the wetting process of the electrode interface by the electrolyte. Afterward, reversible capacities of around 160 mAh $g^{-1}$ are achieved. It is noteworthy that the Li/PEO-$Cs^+$/LFP cell maintains a high and stable CE of around 100% within 100 cycles, while the CE of Li/PEO/LFP cell significantly dropped to 85.0% and 48.5% at the 4th cycle and 6th cycle, respectively, from 100% at the 3rd cycle. Considering that the same anode and cathode is applied in the two cells, such a large difference in CE can be attributed to the different electrolytes in the two cells. A high capacity of around 160 mAh $g^{-1}$ is delivered by the Li/PEO/LFP cell, corresponding to an areal capacity of 0.48 mAh $cm^{-2}$. In contrast, the PEO electrolyte is unable to suppress the Li dendrite formation according to the Li–Li symmetrical cells in Fig. 2. Under this circumstance, a short circuit occurs, which is confirmed by the charge/discharge profiles in Fig. S5. As it can be seen, at the 4th and 6th cycle, a fluctuating charge profile followed by a sudden voltage drop when charging to 100 and 70 mAh $g^{-1}$, respectively, indicates the occurrence of a soft short circuit and results in low CEs [32]. In contrast, no short circuit is observed for the PEO-$Cs^+$/LFP cell and a CE as high as 100% can be retained during the whole charge/discharge process, further demonstrating the strong capability of PEO-$Cs^+$ electrolyte in inhibiting Li dendrite growth. Even after 100 cycles, the Li/PEO-$Cs^+$/LFP cell still retains a capacity of 124 mAh $g^{-1}$. In order to further demonstrate the Li dendrite suppression capability of PEO-$Cs^+$ electrolyte, a high rate of 0.5C is applied for Li/PEO-$Cs^+$/LFP cell testing, corresponding to a high current density of around 0.26 mA $cm^{-2}$. As shown in Fig. 4b, similar to the performance at 0.2C, a reversible capacity of 133 mAh $g^{-1}$ at the 14th cycle is achieved after an activation process. After 100 cycles, a high capacity of around 120 mAh $g^{-1}$ is retained with a high capacity retention of over 90%, showing excellent cycling performance. However, for the Li/PEO/LFP cell, a more serious short-circuit phenomenon at an early stage can be observed with a sudden CE drop to 76.8% at the 3rd cycle. After the 5th cycle, a CE of less than 40% is obtained, which is demonstrated by the charge/discharge profiles in Fig. 4d. The more serious short-circuit and lower CEs for Li/PEO/LFP can be attributed to the more serious Li dendrite growth under high current densities [23,33].

The C-rate performance of Li/PEO/LFP and Li/PEO-$Cs^+$/LFP cells are studied with C-rates ranging from 0.1C to 0.8C. As shown in Fig. 4c, a short circuit occurs in the Li/PEO/LFP cell at the end of the 0.2C testing, where the CE slightly drop to 98.2% at the 8th cycle from 99.6% at the 7th cycle. The short-circuit is further confirmed by the charge/discharge profiles in Fig. 4f. An obvious fluctuating charge profile is observed at the

end of the charge (blue charge profile at 0.2C). When the C-rate is further increased to 0.3C, a more obvious and serious short-circuit can be observed. As displayed by the green charge profile at 0.3C, when charging to around 75 mAh $g^{-1}$, a sudden voltage drop in the fluctuating charge profile appears, suggesting the occurrence of a short-circuit. In this case, a low CE of less than 75% is achieved. These results indicate that the pure PEO electrolyte can't meet the demand of the Li-LFP cells with a LFP loading of 3 mg $cm^{-2}$ in suppressing Li dendrite growth. On the contrary, there is no short circuit phenomenon and high CEs of around 100% are observed for Li/PEO- $Cs^+$/LFP cell during the C-rate performance testing (Fig. 4c and e). The cell delivers average capacities of 163, 160, 152 and 137 mAh $g^{-1}$ at 0.1, 0.2, 0.3 and 0.5C. Even when the C-rate further increases to 0.8C, a high 113 mAh $g^{-1}$ is maintained.

Such large differences in electrochemical performance for Li–Li symmetric cells and Li-LFP cells assembled with PEO and PEO-$Cs^+$ electrolytes highlight that the $Cs^+$ additive is effective in inhibiting Li dendrite growth in ASSLBs based on the SHES mechanism. Considering the extremely low concentration (<1 wt%) and facile process, it shows great potential for practical application in high-performance ASSLBs.

## 4. Conclusions

In summary, we have successfully explored an effective and sustainable electrolyte additive for ASSLBs, which is beneficial for inhibiting Li dendrite growth based on the SHES mechansim. According to the Nernst equation, the $Cs^+$ does not electrodeposit during cycling and preferably forms a positively charged shield, which forces incoming $Li^+$ deposition at the adjacent regions of the anode instead of the Li dendrite tips, resulting in a smooth deposition layer and dendrite-free Li anode surface. Based on this concept, with an extremely low $Cs^+$ concentration of 0.05 M, corresponding to a low weight ratio of less than 1 wt %, the Li–Li symmetric cell can stably run for 1000 h (0.1 mA $cm^{-2}$, 0.1 mAh $cm^{-2}$) and 500 h (0.2 mA $cm^{-2}$, 0.2mAh $cm^{-2}$), respectively, which are almost one order of magnitude longer than pure PEO electrolyte. Additionally, the Li/PEO-$Cs^+$/LFP cell assembled with 3 mg $cm^{-2}$ LFP achieves a high capacity retention of 90% within 100 cycles at 0.5C and a high capacity of 113 mAh $g^{-1}$ remains at 0.8C, while short-circuits can be observed for the Li/PEO/LFP cell even at a low C-rate of 0.2C. Considering the facile process and high-efficiency, this strategy shows promising potential in preventing metal dendrite growth in other SSBs systems such as Li/Na–S and Li/Na–$O_2$ as well as Na-ion batteries.

## Author contributions

X. Yang conceived and designed the experimental work and prepared the manuscript; C. Zhao helped with SEM characterization; X. Gao helped with electrode preparation; Q. Sun, K. Adair, J. Luo, Y. Zhang, X. Lin, J. Liang, H. Huang, L. Zhang, S. Lu, and R. Li participated in the discussion of the data; X. Sun supervised the overall project. All authors have given approval to the final version of the manuscript.

## Acknowledgements

This work was partly supported by Natural Sciences and Engineering Research Council of Canada, Canada Research Chair Program (CRC), Canada Foundation for Innovation, and Western University.

## Appendix A. Supplementary data

Supplementary data to this article can be found online at https://doi.org/10.1016/j.ensm.2019.07.015.

## References

[1] A. Manthiram, X. Yu, S. Wang, Nat. Rev. Mater. 2 (2017) 16103.
[2] Y. Zhao, K. Zheng, X. Sun, Joule 2 (2018) 2583–2604.
[3] E. Umeshbabu, B. Zheng, Y. Yang, Electrochem. Energy Rev. 2 (2019) 199–230.
[4] S.-J. Tan, X.-X. Zeng, Q. Ma, X.-W. Wu, Y.-G. Guo, Electrochem. Energy Rev. 1 (2018) 113–138.
[5] B. Commarieu, A. Paolella, J.-C. Daigle, K. Zaghib, Curr. Opin. Electrochem. 9 (2018) 56–63.
[6] J. Zhang, J. Yang, T. Dong, M. Zhang, J. Chai, S. Dong, T. Wu, X. Zhou, G. Cui, Small 14 (2018), e1800821.
[7] H. Huo, N. Zhao, J. Sun, F. Du, Y. Li, X. Guo, J. Power Sources 372 (2017) 1–7.
[8] X. Yang, X. Li, K. Adair, H. Zhang, X. Sun, Electrochem. Energy Rev. 1 (2018) 239–293.
[9] H. Zhang, J. Zhang, J. Ma, G. Xu, T. Dong, G. Cui, Electrochem. Energy Rev. 2 (2019) 128–148.
[10] W. Zhou, Z. Wang, Y. Pu, Y. Li, S. Xin, X. Li, J. Chen, J.B. Goodenough, Adv. Mater. 31 (2019) 1805574.
[11] S. Liu, N. Imanishi, T. Zhang, A. Hirano, Y. Takeda, O. Yamamoto, J. Yang, J. Electrochem. Soc. 157 (2010) A1092.
[12] C. Wang, Y. Yang, X. Liu, H. Zhong, H. Xu, Z. Xu, H. Shao, F. Ding, ACS Appl. Mater. Interfaces 9 (2017) 13694–13702.
[13] X. Yang, Q. Sun, C. Zhao, X. Gao, K.R. Adair, Y. Liu, J. Luo, X. Lin, J. Liang, H. Huang, L. Zhang, R. Yang, S. Lu, R. Li, X. Sun, Nano Energy 61 (2019) 567–575.
[14] D. Lin, P.Y. Yuen, Y. Liu, W. Liu, N. Liu, R.H. Dauskardt, Y. Cui, Adv. Mater. 30 (2018) 1802661.
[15] C.Z. Zhao, X.Q. Zhang, X.B. Cheng, R. Zhang, R. Xu, P.Y. Chen, H.J. Peng, J.Q. Huang, Q. Zhang, Proc. Natl. Acad. Sci. U.S.A. 114 (2017) 11069–11074.
[16] X.X. Zeng, Y.X. Yin, N.W. Li, W.C. Du, Y.G. Guo, L.J. Wan, J. Am. Chem. Soc. 138 (2016) 15825–15828.
[17] H. Huo, Y. Chen, J. Luo, X. Yang, X. Guo, X. Sun, Adv. Energy Mater. 9 (2019) 1804004.
[18] G.G. Eshetu, X. Judez, C. Li, O. Bondarchuk, L.M. Rodriguez-Martinez, H. Zhang, M. Armand, Angew. Chem. Int. Ed. 56 (2017) 15368–15372.
[19] F. Ding, W. Xu, G.L. Graff, J. Zhang, M.L. Sushko, X. Chen, Y. Shao, M.H. Engelhard, Z. Nie, J. Xiao, X. Liu, P.V. Sushko, J. Liu, J.G. Zhang, J. Am. Chem. Soc. 135 (2013) 4450–4456.
[20] Y. Zhao, R. Tao, T. Fujinami, Electrochim. Acta 51 (2006) 6451–6455.
[21] O. Sheng, C. Jin, J. Luo, H. Yuan, C. Fang, H. Huang, Y. Gan, J. Zhang, Y. Xia, C. Liang, W. Zhang, X. Tao, J. Mater. Chem. A 5 (2017) 12934–12942.
[22] Y. Zhao, X. Yang, L.Y. Kuo, P. Kaghazchi, Q. Sun, J. Liang, B. Wang, A. Lushington, R. Li, H. Zhang, X. Sun, Small 14 (2018) 1703717.
[23] Y. Zhao, X. Yang, Q. Sun, X. Gao, X. Lin, C. Wang, F. Zhao, Y. Sun, K.R. Adair, R. Li, M. Cai, X. Sun, Energy Storage Mater. 15 (2018) 415–421.
[24] S. Wang, X. Liu, A. Wang, Z. Wang, J. Chen, Q. Zeng, X. Jiang, H. Zhou, L. Zhang, ACS Appl. Mater. Interfaces 10 (2018) 25273–25284.
[25] S. Li, Y.-M. Chen, W. Liang, Y. Shao, K. Liu, Z. Nikolov, Y. Zhu, Joule 2 (2018) 1838–1856.
[26] D. Zhang, L. Zhang, K. Yang, H. Wang, C. Yu, D. Xu, B. Xu, L.M. Wang, ACS Appl. Mater. Interfaces 9 (2017) 36886–36896.
[27] X. Judez, H. Zhang, C. Li, G.G. Eshetu, Y. Zhang, J.A. Gonzalez-Marcos, M. Armand, L.M. Rodriguez-Martinez, J. Phys. Chem. Lett. 8 (2017) 3473–3477.
[28] K. Yin, Z. Zhang, X. Li, L. Yang, K. Tachibana, S. Hirano, J. Mater. Chem. A 3 (2015) 170–178.
[29] J. Chai, Z. Liu, J. Ma, J. Wang, X. Liu, H. Liu, J. Zhang, G. Cui, L. Chen, Adv. Sci. 4 (2017) 1600377.
[30] X.B. Cheng, R. Zhang, C.Z. Zhao, Q. Zhang, Chem. Rev. 117 (2017) 10403–10473.
[31] P. Zou, Y. Wang, S.W. Chiang, X. Wang, F. Kang, C. Yang, Nat. Commun. 9 (2018) 464.
[32] F. Gonzalez, P. Tiemblo, N. Garcia, O. Garcia-Calvo, E. Fedeli, A. Kvasha, I. Urdampilleta, Membranes 8 (2018).
[33] H. Wang, D. Lin, Y. Liu, Y. Li, Y. Cui, Sci. Adv. 3 (2017) 1701301.